ACS OMEGA

Open Access



http://pubs.acs.org/journal/acsodf

Article

# Discovery of Novel Naphthoquinone−Chalcone Hybrids as Potent FGFR1 Tyrosine Kinase Inhibitors: Synthesis, Biological Evaluation, and Molecular Modeling

Ronnakorn Leechaisit, Panupong Mahalapbutr,* Pornthip Boonsri, Kun Karnchanapandh, Thanyada Rungrotmongkol, Veda Prachayasittikul, Supaluk Prachayasittikul, Somsak Ruchirawat, Virapong Prachayasittikul, and Ratchanok Pingaew*

Cite This: *ACS Omega* 2023, 8, 32593−32605

Read Online

ACCESS | Metrics & More | Article Recommendations | Supporting Information

**ABSTRACT:** This work presents a flexible synthesis of 10 novel naphthoquinone−chalcone derivatives (**1**−**10**) by nucleophilic substitution of readily accessible aminochalcones and 2,3-dichloro-1,4-naphthoquinone. All compounds displayed broad-spectrum cytotoxic activities against all the tested cancer cell lines (i.e., HuCCA-1, HepG2, A549, MOLT-3, T47D, and MDA-MB-231) with $IC_{50}$ values in the range of 0.81−62.06 $\mu$M, especially the four most potent compounds **1**, **3**, **8**, and **9**. The *in vitro* investigation on the fibroblast growth factor receptor 1 (FGFR1) inhibitory effect indicated that eight derivatives (**1**−**2**, **4**−**5**, and **7**−**10**) were active FGFR1 inhibitors ($IC_{50}$ = 0.33−3.13 nM) with more potency than that of the known FGFR1 inhibitor, AZD4547 ($IC_{50}$ = 12.17 nM). Promisingly, compounds **5** ($IC_{50}$ = 0.33 ± 0.01 nM), **9** ($IC_{50}$ = 0.50 ± 0.04 nM), and **7** ($IC_{50}$ = 0.85 ± 0.08 nM) were the three most potent FGFR1 inhibitors. Molecular docking, molecular dynamics simulations, and MM/GBSA-based free energy calculation revealed that the key amino acid residues involved in the binding of the compounds **5**, **7**, and **9** and the target FGFR1 protein were similar with those of the AZD4547 (i.e., Val492, Lys514, Ile545, Val561, Ala640, and Asp641). These findings revealed that the newly synthesized naphthoquinone−chalcone scaffold is a promising structural feature for an efficient inhibition of FGFR1.

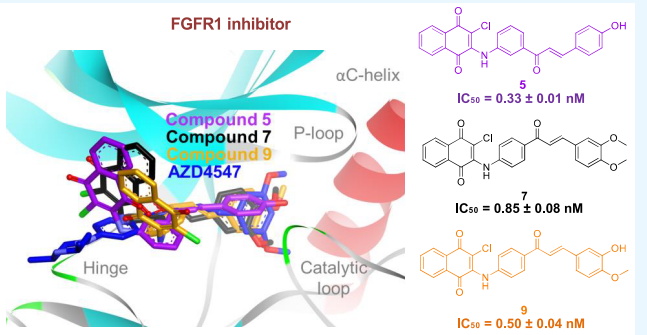


## INTRODUCTION

Cancer has been noted as one of leading causes of death globally, and its impacts on human well-being are well-recognized.[1] While numerous classes of anticancer drugs are currently available for clinical use, their adverse effects and resistance are still of concern as challenging issues for effective management.[2] Hence, the development of novel versatile chemotherapeutic agents to be potentially used as alternative drugs has gained continual interest.[3−5]

Fibroblast growth factor receptors (FGFRs) are a cell membrane-expressing receptor tyrosine kinase family with four subfamily members (FGFR1, FGFR2, FGFR3, and FGFR4). The activation of the FGFRs upon binding of the native ligand leads to various vital physiological processes of the cells, including proliferation, differentiation, migration, and survival. Overexpression of FGFRs is observed in many types of cancers (i.e., urothelial carcinoma, cholangiocarcinoma, endometrial cancer, ovarian cancer, breast cancer, and non-small cell lung cancer).[6−8] Accordingly, the development of FGFR antagonists/inhibitors to counteract the effects of FGFR overactivation has become an attractive therapeutic strategy.[9] Several FGFR antagonists have been developed, and some of them are currently being used in clinical trials or are undergoing preclinical investigations such as LY2874455, ARQ-087, AZD4547, FGF401, BLU9931, and H3B6527s.[10]

The hybridization of bioactive pharmacophores with different mechanisms of action into a single multifunctional molecule is considered an attractive strategy in current rational drug design.[11−16] In addition to their multiple actions, hybrid compounds mostly display simpler and preferable pharmacokinetic profiles, which are essential for further successful drug development.[15] Of note, several hybrid molecules are under different phases of clinical trials and are along the way of approval for treatment of several diseases,[16] including those of problematic cancer drug resistance.[15]

Received: May 8, 2023
Accepted: August 14, 2023
Published: August 30, 2023

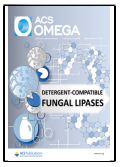

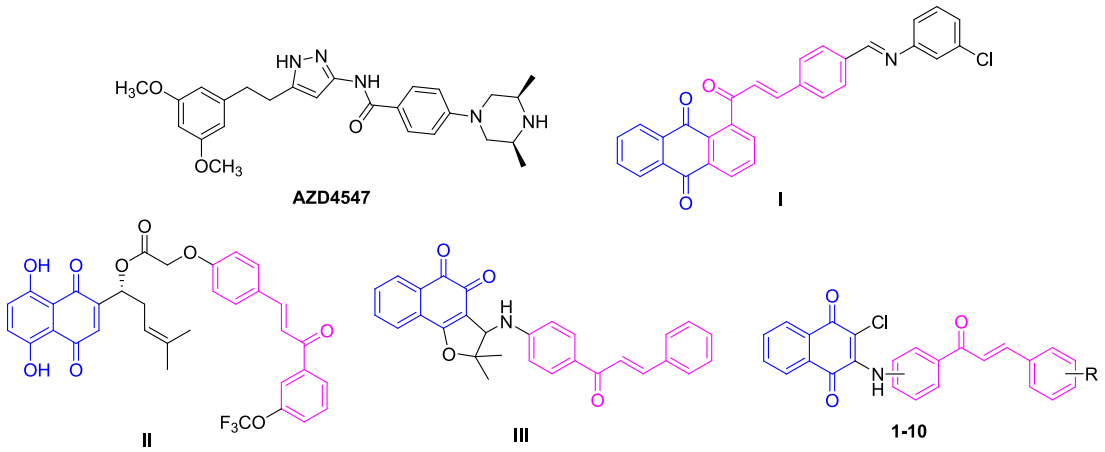


**Figure 1.** Structures of AZD4547 and chalcone−naphthoquinone hybrids: previously reported hybrids **I**−**III** and our synthesized hybrids **1**−**10**.

**Scheme 1. Synthesis of Naphthoquinone−Chalcone Derivatives (1−10)**

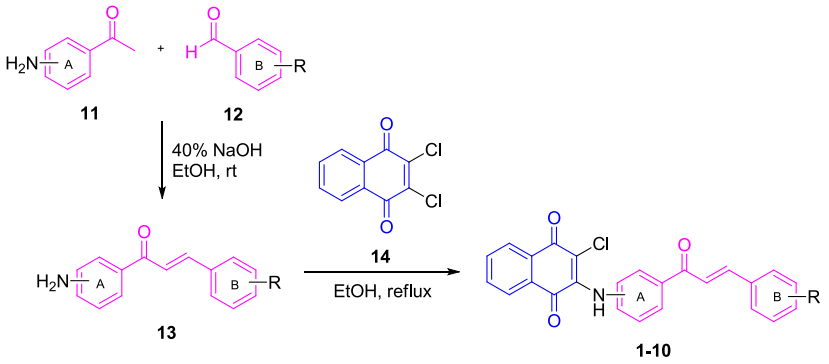


Naturally derived compounds are well-recognized as great sources of pharmacophores and bioactive fragments for potential drug design and development. Chalcones are flavonoid derivatives naturally found in many edible plants and spices. Chalcone derivatives were reported for their wide-ranging biological activities, including anticancer effects.[17−20] Additionally, various mechanisms of action underlying the anticancer properties of the chalcone-based compounds have been reported.[21,22] Quinone is a core skeleton present in several classes of naturally occurring bioactive compounds, and their analogs have been clinically used as anticancer drugs (i.e., daunorubicin, doxorubicin, and mitoxantrone).[23,24] The 1,4-naphthoquinone scaffold is a privileged structure containing two ketone groups as crucial moieties contributing to its chelating and electrochemical properties.[25,26] Apparently, an ability to accept electrons is noted to be an essential key property for broad-ranging biological activities of naphthoquinone derivatives.[27,28]

The pharmacological significance of chalcone and naphthoquinone scaffolds has inspired the scientific community to synthesize hybrid molecules based on these skeletons to provide diverse biological activities.[29−35] The hybridization of these moieties (chalcone and naphthoquinone) into a single molecule has been reported in the literature.[36−39] For example, chalcone−naphthoquinone hybrids **I**−**III** (Figure 1) possessing anticancer activity have been studied.[37−39] The anthraquinone-based chalcone **I** showed potent activity against HeLa, LS174, and A549 cancer cell lines ($IC_{50}$ = 1.93−17.18 $\mu$M) and exhibited strong antiangiogenic activity.[37] Shikonin-based chalcone **II** showed potent anticancer and antitubulin effects against HeLa, MCF-7, and A549 cancer cell lines ($IC_{50}$ = 2.36−5.84 $\mu$M).[38] Nor-$\beta$-lapachone-based chalcone **III** displayed potent cytotoxic activities against four cancer cell lines (HL-60, OVCAR-8, SF295, and HCT-116) affording the $IC_{50}$ range of 0.04−1.53 $\mu$M.[39] These reports suggested that the two pharmacophores are potential core skeletons for the synthesis of hybrid multifunctional compounds. However, there are only a few examples of chalcone−naphthoquinone conjugates that have been explored, and their molecular targets underlying the anticancer properties are rarely understood.

Computational tools are widely recognized for their roles in facilitating successful drug development. Molecular docking and molecular dynamics are structural-based methods to elucidate the binding nature and key binding interactions between the compounds and their biological targets.[40] They are beneficial key knowledge for further design and development of the related compounds with improved activity and properties. Currently, some examples of the modeling for revealing binding modes of the epidermal growth factor receptor (EGFR) inhibitors have been published by our research group.[41]

In this study, a novel set of chalcone−naphthoquinone hybrids **1**−**10** (Figure 1) was synthesized and investigated for their *in vitro* anticancer effects against 6 cancer cell lines as well as FGFR1 inhibitory activity. Furthermore, molecular docking and molecular dynamics simulations were performed to reveal possible binding modalities and ligand−target interactions.



https://doi.org/10.1021/acsomega.3c03176
*ACS Omega* 2023, 8, 32593−32605

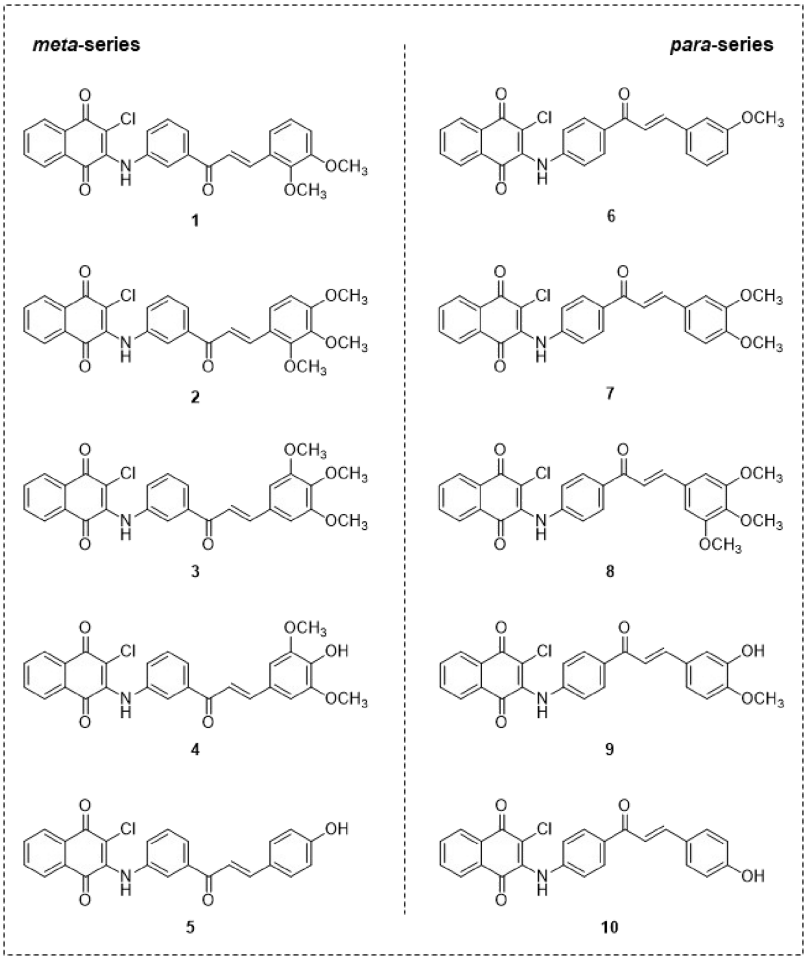


**Figure 2.** Chemical structures of naphthoquinone−chalcone derivatives (**1**−**10**).

## RESULTS AND DISCUSSION

**Chemistry.** The new naphthoquinone−chalcone derivatives (**1**−**10**) were synthesized in two-step reactions as shown in Scheme 1. Initially, aminochalcones **13** were readily prepared by base-catalyzed Claisen−Schmidt condensation of benzaldehyde derivatives **12** with 3- or 4-aminoacetophenone **11** in the presence of 40% NaOH in ethanol at room temperature.[35,42] Then, the target hybrids **1**−**10** were obtained by a nucleophilic substitution reaction[34,41] of chalcones **13** with 2,3-dichloro-1,4-naphthoquinone (**14**) in refluxing ethanol (35−58% yields). Structures of the hybrids **1**−**10** were characterized by $^{1}$H NMR, $^{13}$C NMR, and HRMS data. $^{1}$H NMR spectra showed a pair of doublets of olefinic protons with the coupling constant ($J$) values of 15−16 Hz representing that the *trans*-configuration was denoted. Additionally, protons of secondary amine substituted on ring A were displayed at $\delta$ 9−10 ppm, indicating that the nucleophilic displacement occurred to form the hybrids **1**−**10**. In $^{13}$C NMR spectra, the three carbonyl groups were observed at $\delta$ 177 to 190 ppm. The central ring A of compounds **1**−**10** was noted as *meta* (**1**−**5**) and *para* (**6**−**10**) isomers (Figure 2).

**Biological Activities.** *Cytotoxic Activity.* Cytotoxic activities of chalcone−naphthoquinone hybrids (**1**−**10**) were investigated against 6 human cancer cell lines, namely, HuCCA-1 (cholangiocarcinoma), HepG2 (hepatocellular carcinoma), A549 (lung carcinoma), MOLT-3 (lymphoblastic leukemia), T47D (hormone-dependent breast cancer), and MDA-MB-231 (hormone-independent breast cancer) cell lines as summarized in Table 1.

In overview, all studied compounds showed a broad anticancer potential against 6 cancer cell lines ($IC_{50}$ value range = 0.81−62.06 $\mu$M), except for the *para*-derivative **9** (inactive against HepG2 and A549 cell lines), while **7** was inactive against the HepG2 cell line. Notably, compounds from the *meta*-series were shown to be more promising compounds than those from the *para*-series as seen from the most potent compounds **1** against three cancer cell lines (i.e., HuCCA-1, HepG2, and A549) and **3** against two breast cancer cell lines (i.e., T47D and MDA-MB-231). Conversely, compounds from the *para*-series (**8** and **9**) were noted to be effective against the MOLT-3 cell line. Most of the potent compounds showed lesser potencies than the reference drug doxorubicin. However, there is an exception for those of the top three most potent compounds (**1**, **3**, and **8**) against the MDA-MB-231 cell line, which displayed lower $IC_{50}$ values compared to doxorubicin.

Compound **1**, a 2,3-di-OMe analog of the *meta*-series, is the most potent compound against the HuCCA-1 cell line ($IC_{50}$ = 1.16 $\mu$M). The second most potent compounds **3** and **8** (3,4,5-tri-OMe analogs of the *meta*- and *para*-series) exhibited equal potency ($IC_{50}$ = 4.72 $\mu$M) followed by compound **5**, a 4-OH analog of the *meta*-series ($IC_{50}$ = 5.65 $\mu$M). It was shown that the replacement of an OMe group substituted on the ring B with the OH group leads to decreased activity for the *meta*-series (compounds **3** > **4**, $IC_{50}$: **3** = 4.72, **4** = 7.06 $\mu$M) but enhanced activity for the *para*-series (compounds **9** > **7**, $IC_{50}$:


https://doi.org/10.1021/acsomega.3c03176
ACS Omega 2023, 8, 32593−32605

Table 1. Cytotoxic Activity ($IC_{50}$, $\mu$M) of Chalcone−Naphthoquinone Derivatives (1−10)

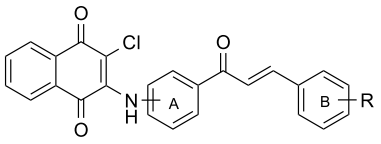


1-10

| Compound | NH of A-ring | R of B-ring |
|---|---|---|
| 1 | 3- | 2,3-di$OCH_3$ |
| 2 | 3- | 2,3,4-tri$OCH_3$ |
| 3 | 3- | 3,4,5-tri$OCH_3$ |
| 4 | 3- | 4-OH-3,5-di$OCH_3$ |
| 5 | 3- | 4-OH |
| 6 | 4- | 3-$OCH_3$ |
| 7 | 4- | 3,4-di$OCH_3$ |
| 8 | 4- | 3,4,5-tri$OCH_3$ |
| 9 | 4- | 3-OH-4-$OCH_3$ |
| 10 | 4- | 4-OH |

| Compound | Cytotoxic activity[e] | | | | | | |
|---|---|---|---|---|---|---|---|
| | HuCCA-1 | HepG2 | A549 | MOLT-3 | T47D | MDA-MB-231 | MRC-5 |
| 1 | 1.16 ± 0.40[a] | 5.13 ± 0.15[a] | 6.12 ± 1.56[a] | 1.24 ± 0.03 | 1.81 ± 0.04[c] | 1.08 ± 0.12[b] | 4.96 ± 0.14 |
| 2 | 8.87 ± 1.03 | 16.29 ± 0.44 | 33.50 ± 0.17 | 1.81 ± 0.05 | 2.32 ± 0.08 | 1.79 ± 0.12 | 2.60 ± 0.04 |
| 3 | 4.72 ± 0.48[b] | 16.91 ± 0.74 | 51.55 ± 10.34 | 0.99 ± 0.12[c] | 1.15 ± 0.08[a] | 1.05 ± 0.04[a] | 2.52 ± 0.26 |
| 4 | 7.06 ± 1.36 | 12.82 ± 0.42 | 24.96 ± 4.22[c] | 1.10 ± 0.14 | 2.12 ± 0.11 | 1.43 ± 0.11 | 2.90 ± 0.48 |
| 5 | 5.65 ± 0.08[c] | 13.07 ± 0.12 | 31.94 ± 3.71 | 2.19 ± 0.26 | 5.75 ± 0.00 | 3.33 ± 0.08 | 10.96 ± 0.99[d] |
| 6 | 11.06 ± 0.37 | 6.88 ± 2.72[b] | 13.54 ± 1.49[b] | 1.78 ± 0.06 | 2.10 ± 0.12 | 1.31 ± 0.03 | 2.69 ± 0.15 |
| 7 | 7.32 ± 0.37 | NC[g] | 62.06 ± 0.14 | 1.27 ± 0.12 | 1.86 ± 0.06 | 1.16 ± 0.03 | 2.93 ± 0.16 |
| 8 | 4.72 ± 0.33[b] | 10.87 ± 0.01[c] | 25.76 ± 3.55 | 0.81 ± 0.02[a] | 1.61 ± 0.07[b] | 1.09 ± 0.02[c] | 2.92 ± 0.36 |
| 9 | 6.85 ± 1.20 | NC[g] | NC[g] | 0.83 ± 0.01[b] | 24.05 ± 1.61 | 6.81 ± 0.52 | 14.94 ± 0.09[d] |
| 10 | 7.70 ± 2.85 | 57.51 ± 1.28 | 44.15 ± 4.06 | 2.35 ± 0.39 | 3.21 ± 0.06 | 1.37 ± 0.07 | 8.31 ± 3.30 |
| etoposide[f] | ND[g] | 33.98 ± 0.01 | ND[g] | 0.041 ± 0.003 | ND[g] | ND[g] | ND[g] |
| doxorubicin[f] | 0.42 ± 0.02 | 0.57 ± 0.05 | 0.37 ± 0.02 | ND[g] | 0.84 ± 0.01 | 1.84 ± 0.13 | 2.79 ± 0.11 |

[a]The most potent compound. [b]The second most potent compound. [c]The third most potent compound. [d]Two compounds with the least cytotoxicity. [e]Cell lines: the HuCCA-1 cholangiocarcinoma cell line, HepG2 hepatocellular carcinoma cell line, A549 lung carcinoma cell line, MOLT-3 lymphoblastic leukemia cell line, T47D hormone-dependent breast cancer, MDA-MB-231 hormone-independent breast cancer, and MRC-5 normal embryonic lung cell line. [f]Doxorubicin and etoposide were used as reference drugs. [g]NC: noncytotoxic = $IC_{50}$ > 50 $\mu$g/mL denoted as noncytotoxic; ND: not determined.

**7** = 7.32, **9** = 6.85 $\mu$M). The significance of the *meta*-amino position on ring A was also noted when the decreased activity was observed for the 4-OH *para*-analog **10** when compared to its *meta*-compound **5** (**5** > **10**, $IC_{50}$: **5** = 5.65, **10** = 7.70 $\mu$M).

Eight out of 10 compounds were active against the HepG2 cell line, in which compound **1** ranked as the most potent one followed by compounds **6** and **8**. Additionally, seven compounds (**1**−**6** and **8**) showed higher potency against the HepG2 cell line ($IC_{50}$ = 5.13−16.91 $\mu$M) than that of the etoposide ($IC_{50}$ = 33.98 $\mu$M). It was demonstrated that the number and position of the OMe group on ring B influenced the activities of the compounds of both series. Notable impaired activities were observed when adding another an OMe group onto the ring B of *meta*-compound **1** ($IC_{50}$ = 5.13 $\mu$M) to give compounds **2** and **3** ($IC_{50}$ = 16.29 and 16.91 $\mu$M, respectively). A similar effect was noted for the *para*-compounds **6**, **7**, and **8** ($IC_{50}$ = 6.88, inactive, and 10.87 $\mu$M, respectively).

Similar patterns of potency were observed for the A549 cell line in which compounds **1** and **6** were ranked as the two most potent compounds, and decreased activities were observed when additional OMe or OH groups were introduced on the ring B of *meta*-analogs (**1** > **2** > **3** and **1** > **4**) as well as *para*-analogs (**6** > **8** > **7**).

Additionally, results revealed that this class of compounds was more sensitive to the MOLT-3 cell line, as shown by the narrow and low $IC_{50}$ range (0.81−2.35 $\mu$M), in which the *para*-compounds **8** and **9** were ranked as the two most potent ones followed by the *meta*-compound **3** ($IC_{50}$: **8** = 0.81, **9** = 0.83, and **3** = 0.99 $\mu$M).

Compounds **1**, **3**, and **8** were noted as the top three most potent compounds for both tested breast cancer cell lines (i.e., T47D and MDA-MB-23). Notably, these three compounds were more potent than doxorubicin ($IC_{50}$ = 1.84 $\mu$M) displaying comparable $IC_{50}$ values against the MDA-MB-23 cell line ($IC_{50}$: **3** = 1.05 > **1** = 1.08 > **8** = 1.09 $\mu$M). For the T47D cell line, these compounds were less potent than doxorubicin ($IC_{50}$ = 0.84 $\mu$M) showing the $IC_{50}$ ranking as **3** = 1.15 > **8** = 1.61 > **1** = 1.81 $\mu$M.

Taken together, the substitution of multiple OMe groups on the B ring was noted to be essential for potent cytotoxic activity of the naphthoquinone−chalcones as observed from the three most potent compounds (i.e., di-OMe compound **1** and tri-OMe compounds **3** and **8**). This is presumably due to the enhanced lipophilic effect of OMe groups required for interacting with the target site of action.

Cytotoxicity investigation against the normal embryonic lung (MRC-5) cell line indicated that compounds **5** ($IC_{50}$ = 10.96 $\mu$M) and **9** ($IC_{50}$ = 14.94 $\mu$M) were the two least cytotoxic compounds followed by compounds **10** ($IC_{50}$ = 8.31 $\mu$M) and **1** ($IC_{50}$ = 4.96 $\mu$M). The rest of the compounds (**2**, **3**, **4**, **6**, **7**, and **8**; $IC_{50}$ = 2.52−2.93 $\mu$M) showed comparable $IC_{50}$ values with that of the reference drug doxorubicin ($IC_{50}$ = 2.79 $\mu$M) (Table 1).



https://doi.org/10.1021/acsomega.3c03176
ACS Omega 2023, 8, 32593−32605

*FGFR Kinase Activity.* The FGFR1 inhibitory activity of 10 naphthoquinone−chalcone compounds (**1**−**10**) was evaluated using the ADP-Glo kinase assay. The known FGFR1 inhibitor AZD4547 was used as a reference drug. The preliminary screening of the compounds at 1 $\mu$M indicated that only eight compounds (**1**, **2**, **4**, **5**, and **7**−**10**) showed active inhibitory effects with % inhibition greater than 70 (Figure S1). Therefore, these compounds were selected for further $IC_{50}$ determination.

Results showed that the selected compounds inhibited FGFR1 kinase activity in a dose-dependent manner affording $IC_{50}$ values in the nanomolar scale (Figure S2 and Table 2).

**Table 2. $IC_{50}$ Values of Naphthoquinone−Chalcones (1−10) and AZD4547 against FGFR1 Tyrosine Kinase**

| compound | $IC_{50}$ (nM)[a] |
|---|---|
| **1** | 0.91 ± 0.08 |
| **2** | 1.50 ± 0.28 |
| **4** | 0.96 ± 0.05 |
| **5** | 0.33 ± 0.01* |
| **7** | 0.85 ± 0.08*** |
| **8** | 1.69 ± 0.71 |
| **9** | 0.50 ± 0.04** |
| **10** | 3.13 ± 0.67 |
| AZD4547 | 12.17 ± 1.35 |

[a]Data are shown as means ± SEM ($n$ = 3). *The most potent compound, **the second most potent compound, and ***the third most potent compound.

The compounds were ranked regarding their potencies as **5** > **9** > **7** > **1** > **4** > **2** > **8** > **10**. Interestingly, the synthesized compounds showed considerably higher potency than the known FGFR1 inhibitor, AZD4547. Of note, the top three most potent compounds including **5**, **9**, and **7** ($IC_{50}$ = 0.33, 0.50, and 0.85 nM, respectively) exhibited higher inhibitory activity than the reported FGFR1 inhibitors such as 3,5-disubstituted indolin-2-ones A13 ($IC_{50}$ = 6.99 nM),[43] 3-vinylquinoxalin-2(1*H*)-ones ($IC_{50}$ = ∼15,000−26,000 nM),[44] 2-arylbenzothiazoles ($IC_{50}$ = 190−370 nM),[45] and indazole 1 ($IC_{50}$ = 100 nM).[46] Accordingly, these three compounds were selected for further *in silico* studies.

**Molecular Modeling.** *Molecular Docking.* Molecular docking was conducted to reveal possible binding modes of compounds **5**, **7**, and **9** against the target protein FGFR1 tyrosine kinase domain (PDB ID 7WCL). Results revealed that these compounds could occupy within an adenosine triphosphate (ATP)-binding pocket of the FGFR1 in a similar manner to the known FGFR1 inhibitor, AZD4547 (Figure 3). The phenyl ring B of the studied compounds (**5**, **7**, and **9**) was pointed to the $\alpha$C-helix to mimic the 3,5-dimethoxyphenyl moiety of the AZD4547, while their naphthoquinone ring was placed near the hinge region of the FGFR1 tyrosine kinase domain.

The 2D protein−ligand interaction profiles were further constructed to unravel the ligand−protein interactions (Figure 4). Results revealed that the interacting amino acid residues involved in the binding of compounds **5**, **7**, and **9** were similar with those of AZD4547, especially the residues Val492, Lys514, Ile545, Val561, Ala640, and Asp641 that interacted with the terminal phenyl ring of the ligands *via* van der Waals and $\pi$ interactions. It should be noted that the number of hydrogen bonds of compound **9** containing the 3-OH group

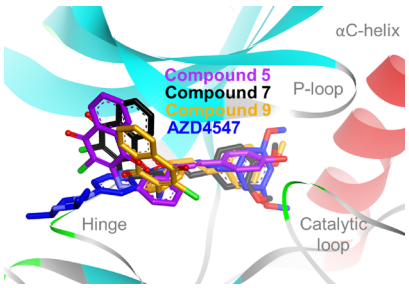


**Figure 3.** Alignment of the docked compounds **5** (purple), **7** (black), and **9** (orange) inside the ATP-binding pocket of the FGFR1 tyrosine kinase domain. The binding orientation of crystallized AZD4547 (blue) was used as the reference.

on the phenyl ring B (two bonds with Asp641 and Asn659 residues) and compound **5** with the 4-OH group on the ring B (three bonds with Lys482, Lys514, and Glu531 residues) was higher than that of the compound **7** without the OH moiety on the phenyl ring B (one bond with the Ala564 residue). Such a high number of hydrogen bonds of **5** may involve the *para*-effect of the phenolic (OH) group contributing the resonance effect to the conjugated keto group (**5** with *p*-OH > **9** with *m*-OH). This could be one of the reasons supporting the higher inhibitory effects of these two compounds (**5** and **9**) beyond the compound **7** (Table 2).

*System Stability.* The stability of compounds **5**, **7**, and **9** in complex with the FGFR1 tyrosine kinase domain along the simulation times was characterized using root-mean-square displacement (RMSD), number of native and non-native contacts (# contacts), and solvent-accessible surface area (SASA) calculations. The RMSD values of the compound **7**/FGFR1 complex were stable at ∼2.5 Å after the first 20 ns, whereas those of compound **5**/FGFR1 and compound **9**/FGFR1 complexes were stable at ∼2.0 Å from the beginning to the end of simulation, reflecting the high stability in an aqueous environment (Figure 5). The # contacts of compound **9**/FGFR1 (18.26 ± 4.77, averaged from the last 20 ns simulation) and compound **5**/FGFR1 (15.83 ± 3.94) complexes were higher than that of the compound **7**/FGFR1 (11.41 ± 4.40) system. This was supported by the lower SASA values on the amino acid residues within 5 Å of compounds **9** and **5** when compared to that of compound **7**. These simulation results were in line with the findings from the *in vitro* FGFR1 kinase assay, which showed that compounds **5** and **9** elicited a better inhibitory effect than compound **7** (Table 2).

*Key Binding Residues.* The key interacting amino acid residues involved in the binding of the studied compounds (**5**, **7**, and **9**) to the target FGFR1 were identified using the per-residue decomposition free energy ($\Delta G_{bind,res}$) calculation based on the molecular mechanics/generalized Born surface area (MM/GBSA) method. The contributing amino acids were colored according to their $\Delta G_{bind,residue}$ values, in which only the residues exhibiting an energy stabilization value of ≤ −1 kcal/mol were focused.

Results revealed that there were five, ten, and seven hotspot residues associated with the binding of compounds **7** (Leu484, Val492, Gly567, Asn568, and Leu630), **9** (Leu484, Gly485, Val492, Lys514, Ile545, Tyr563, Ala564, Leu630, Ala640, and Asp641) and **5** (Leu484, Val492, Lys514, Glu531, Val561, Asn568, and Leu630), respectively (Figure 6). The findings agreed with those obtained from the # contacts (Figure 6) and


https://doi.org/10.1021/acsomega.3c03176
ACS Omega 2023, 8, 32593−32605

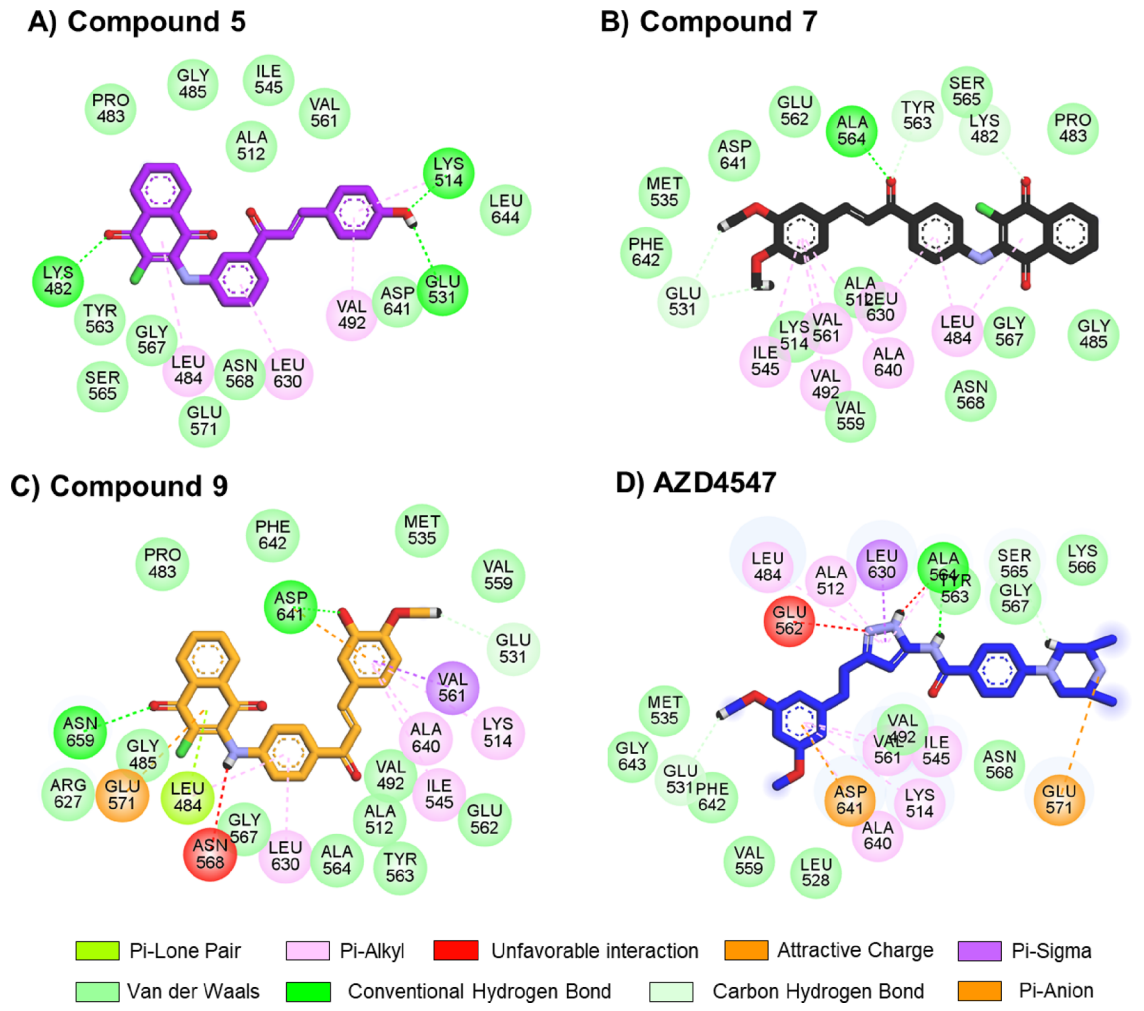


**Figure 4.** Two-dimensional ligand−protein interaction profiles of three investigated naphthoquinone−chalcones in complex with FGFR1; (A) compound **5**, (B) compound **7**, (C) compound **9**, and (D) cocrystallized AZD4547.

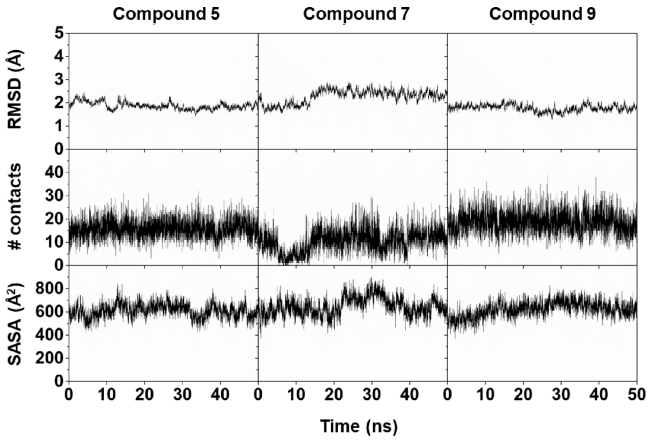


**Figure 5.** Time evolution of RMSD (top), # contacts (middle), and SASA (bottom) of compounds **5**, **7**, and **9** in complex with the FGFR1 tyrosine kinase domain.

*in vitro* assay (Table 2). These interacting amino acid residues were also noted for other reported FGFR1 inhibitors such as 1-(1*H*-benzimidazol-5-yl)-5-aminopyrazoles,[47] 2-arylbenzothiazoles,[45] and indazole 1.[46] The van der Waals ($\Delta E_{vdW}$ + $\Delta G_{solv,nonpolar}$) and electrostatic ($\Delta E_{elec}$ + $\Delta G_{solv,polar}$) contributions from each interacting residue of FGFR1 to the bindings of compounds **5**, **7**, and **9** were further investigated. It was demonstrated that the main energy contributing to the binding of naphthoquinone−chalcone analogs against the target FGFR1 residues is the van der Waals interactions (blue line) rather the electrostatic attraction (red line) (Figure 7). However, the high electrostatic contribution was found between (i) the Asp641 residue and compound **9** as well as (ii) the Glu531 residue and compound **5**, which was due to the strong hydrogen bond formation between them (almost 100% occupation, Figure 8).

*Druglikeness Prediction.* The druglike properties of three selected compounds (**5**, **7**, and **9**) along with the known FGFR1 inhibitor (AZD4547) were predicted using the SwissADME web tool.[48] The investigated properties include the molecular weight (MW), number of hydrogen bond donors (HBD) and acceptors (HBA), number of rotatable bonds (RB), topological polar surface area (TPSA), and lipophilicity (LogP). The predictions demonstrated that all investigated compounds (**5**, **7**, and **9**) are druglike compounds as shown by their predicted parameter values falling within the range of Lipinski's rule of five criteria: (i) MW ≤ 500 Da, (ii) HBD ≤ 5 and HBA ≤ 10, (iii) RB ≤ 10, (iv) TPSA ≤ 140 Å$^2$, and (v) LogP ≤ 5 (Table 3). This suggested that these three synthesized compounds have potential to be developed as novel anticancer drugs.



https://doi.org/10.1021/acsomega.3c03176
ACS Omega 2023, 8, 32593−32605

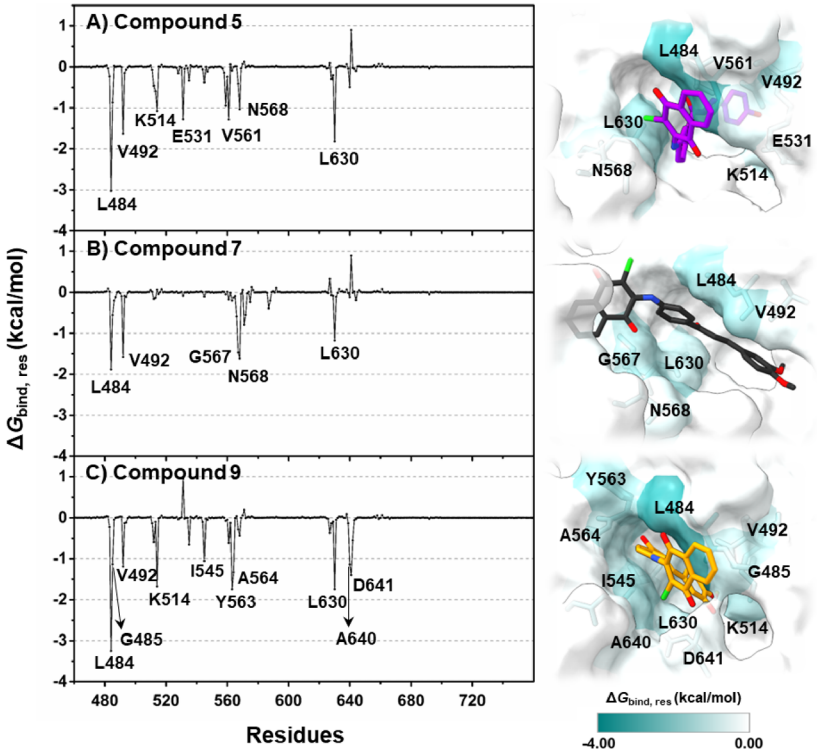


**Figure 6.** (Left) $\Delta G_{bind,residue}$ of (A) compound **5**, (B) compound **7**, and(C) compound **9** in complex with the FGFR1 tyrosine kinase domain. (Right) Representative 3D structures showing the orientation of ligands in the ATP-binding site drawn from the last MD snapshot.

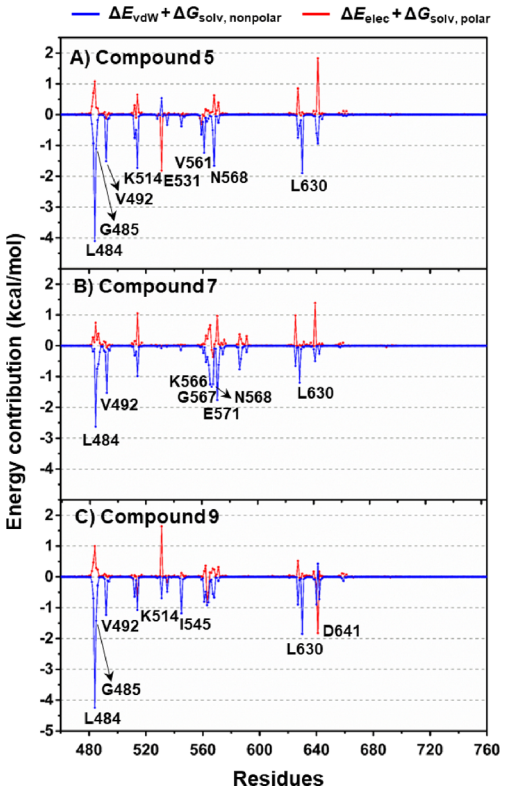


**Figure 7.** Energy contribution from electrostatic ($\Delta E_{elec}$ + $\Delta G_{solv,polar}$, red line) and van der Waals ($\Delta E_{vdW}$ + $\Delta G_{solv,nonpolar}$, blue line) terms from each residue of FGFR1 to the binding of (A) compound **5**, (B) compound **7**, and (C) compound **9**.

## CONCLUSIONS

The nucleophilic substitution reaction utilizing readily available aminochalcones **13** and 2,3-dichloro-1,4-naphthoquinone **14** has been developed to obtain a set of novel naphthoquinone−chalcone derivatives (**1**−**10**). All the synthesized compounds exhibited broad-ranging anticancer activities against 6 cancer cell lines ($IC_{50}$ = 0.81−62.06 $\mu$M). Compounds **1**, **3**, **8**, and **9** were highlighted as promising anticancer agents. Results from the FGFR1 inhibitory screening assay indicated that eight derivatives (**1**−**2**, **4**−**5**, and **7**−**10**) are active FGFR1 inhibitors ($IC_{50}$ = 0.33−3.13 nM) with higher potency than that of the known FGFR1 inhibitor, AZD4547 ($IC_{50}$ = 12.17 nM). Three compounds (**5**, **7**, and **9**) were noted as the three most potent FGFR1 inhibitors and were further selected for *in silico* investigations. Molecular docking indicated that these three compounds (**5**, **7**, and **9**) could snugly occupy within the ATP-binding pocket of the target protein FGFR1 in a similar manner as well as shared key interacting amino acid residues with the AZD4547 (i.e., Val492, Lys514, Ile545, Val561, Ala640, and Asp641 residues). The ligand−protein interaction diagrams revealed that additional hydrogen bonding formation between compounds **9** and **5** and the FGFR1 would play a role for their superior inhibitory effects beyond the compound **7**. Molecular dynamics simulations also suggested that the bindings of these compounds were mainly contributed from the van der Waals interactions. Additionally, these top three FGFR1 inhibitors (**5**, **7**, and **9**) were predicted as druglike compounds with considerable potential for further development. Finally, a novel set of naphthoquinone−chalcone derivatives was suggested to be potentially developed as anticancer candidates (**1**, **3**, **8**, and **9**) as well as FGFR1 inhibitors (**5**, **7**, and **9**) for cancer management, in which compounds **9** and **5** were


https://doi.org/10.1021/acsomega.3c03176
ACS Omega 2023, 8, 32593−32605

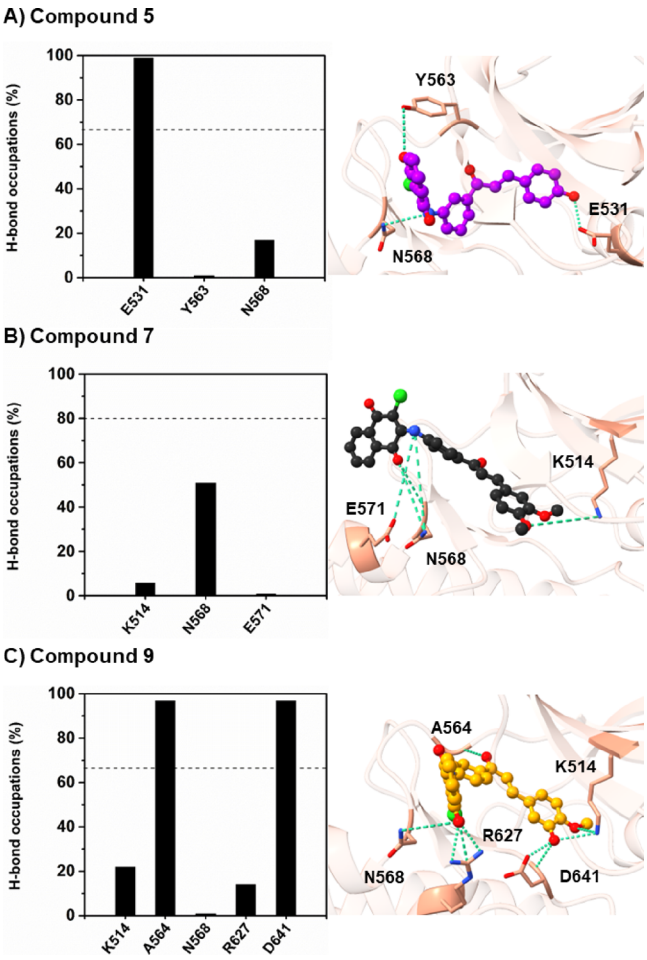


**Figure 8.** Percentage of H-bond occupation of FGFR1 contributing to the binding of (A) compound **5**, (B) compound **7**, and (C) compound **9**, where the ligand orientation in the enzyme active site is illustrated in the right panel.

highlighted as the most promising ones with a preferable safety profile (showing the least cytotoxicity against the normal cell MRC-5).

## EXPERIMENTAL SECTION

**Chemistry.** Column chromatography was carried out using silica gel 60 (70−230 mesh ASTM). Analytical thin-layer chromatography (TLC) was performed on silica gel 60 $F_{254}$ aluminum sheets. Melting points were determined using a Griffin melting point apparatus and were uncorrected. $^1$H and $^{13}$C NMR spectra were recorded on a Bruker AVANCE 300 NMR spectrometer or a Bruker AVANCE NEO 500 NMR spectrometer. Fourier transform infrared spectra were obtained using universal attenuated total reflectance attached on a PerkinElmer Spectrum One spectrometer. High-resolution mass spectra (HRMS) were recorded on a Bruker Daltonics (microTOF). High-performance liquid chromatography (HPLC) was carried out using a Waters 600 pump and controller, a 717 autosampler, equipped with a 996 PDA detector at 360 nm, a column (Nova-Pak, C18, 4 $\mu$m, 60 Å, 150 mm × 3.9 mm), and mobile phases: $H_2O$ (A) and acetonitrile (B); conditions: isocratic at 60% B and 40% A, a flow rate of 1 mL/min, a running time of 10 min, and an injection volume of 10.00 $\mu$L. Each sample was prepared in acetonitrile/water (9/1).

All biological tested compounds **1**−**10** were of >95% purity as determined by HPLC, except for compound **6** that showed 92% purity.

**General Procedure for the Synthesis of Aminochalcones (13).** Compounds **13** were synthesized using previously reported methods[35,42] with minor modifications. A mixture of aminoacetophenone **11** (6 mmol) and benzaldehyde derivative **12** (6 mmol) in ethanol (15 mL) was stirred at 4 °C; then, 40% NaOH (5 mL) was added dropwise. The reaction mixture was stirred at room temperature and monitored by TLC until the completion of the reaction. The reaction mixture was neutralized with 2 M HCl; then, the precipitate was filtered and washed with cold water and cold ethanol to give compound **13**. In the case of (*E*)-1-(3-aminophenyl)-3-(2,3-dimethoxyphenyl)prop-2-en-1-one, the reaction mixture was neutralized with 2 M HCl after completion of the reaction. The mixture was extracted with ethyl acetate (3 × 30 mL). The combined organic phases were washed with water (25 mL), dried over anhydrous sodium sulfate, and evaporated to dryness. The crude product was purified using silica gel column chromatography. $^1$H and $^{13}$C NMR spectra of the aminochalcone derivatives **13** were consistent with those reported in the literature.

**General Procedure for the Synthesis of Naphthoquinone−Chalcone Derivatives (1−10).** A mixture of 2,3-dichloro-1,4-naphthoquinone **14** (2.4 mmol) and the appropriate aminochalcone derivative **13** (2.0 mmol) in absolute ethanol (20 mL) was stirred under reflux until completion of the reaction as monitored by TLC and then concentrated under reduced pressure. The crude product was purified using silica gel column chromatography to afford the pure product.

*(E)-2-Chloro-3-((3-(3-(2,3-dimethoxyphenyl)acryloyl)-phenyl)amino)naphthalene-1,4-dione (Compound 1).* From 2,3-dichloro-1,4-naphthoquinone and (*E*)-1-(3-aminophenyl)-3-(2,3-dimethoxyphenyl)prop-2-en-1-one. Orange solid. 48% yield; mp 213−215 °C; IR (neat) cm$^{-1}$: 3204, 1677, 1600, 1571. $^1$H NMR (500 MHz, DMSO-$d_6$): $\delta$ 3.79, 3.84 (2 s, 6H,

**Table 3. Predicted Values of Druglikeness Parameters According to Lipinski's Rule of Five Criteria for Compounds 5, 7, 9, and AZD4547**[a]

| | Lipinski's rule of five | | | | | | |
|---|---|---|---|---|---|---|---|
| compound | MW (≤500 Da) | HBD (≤5) | HBA (≤10) | RB (≤10) | TPSA (≤140 Å$^2$) | MLogP (≤5) | druglikeness |
| **5** | 429.85 | 2 | 4 | 5 | 83.47 | 2.13 | yes |
| 7 | 473.90 | 1 | 5 | 7 | 81.70 | 1.99 | yes |
| **9** | 459.88 | 2 | 5 | 6 | 92.70 | 1.79 | yes |
| AZD4547 | 463.57 | 3 | 5 | 9 | 91.51 | 2.48 | yes |

[a]MW, molecular weight; HBD, number of hydrogen bond donors; HBA, number of hydrogen bond acceptors; RB, number of rotatable bonds; TPSA, topological polar surface area; LogP, lipophilicity.



https://doi.org/10.1021/acsomega.3c03176
ACS Omega 2023, 8, 32593−32605

2 × $OCH_3$), 7.12−7.17 (m, 2H, Ar*H*), 7.42 (dd, *J* = 8.0, 1.2 Hz, 1H, Ar*H*), 7.51 (t, *J* = 7.8 Hz, 1H, Ar*H*), 7.56 (dd, *J* = 6.9, 2,3 Hz, 1H, Ar*H*), 7.81−7.90 (m, 5H, Ar*H*, COC*H*═CHAr), 7.98 (d, *J* = 15.8 Hz, 1H, COCH═C*H*Ar), 8.06 (dd, *J* = 7.7, 0.9 Hz, 2H, Ar*H*), 9.46 (s, 1H, N*H*). $^{13}$C NMR (125 MHz, DMSO-$d_6$): δ 55.9, 61.0, 115.2, 115.3, 119.3, 122.9, 123.3, 124.3, 124.4, 126.2, 126.6, 128.1, 128.2, 128.5, 130.4, 131.9, 133.4, 134.8, 137.5, 138.3, 139.6, 143.1, 148.3, 152.8, 176.9, 180.1, 189.0. HRMS-TOF: [M + H]$^+$, 474.1103 (calcd for $C_{27}H_{21}ClNO_5$: 474.1103).

*(E)-2-Chloro-3-((3-(3-(2,3,4-trimethoxyphenyl)acryloyl)-phenyl)amino)naphthalene-1,4-dione (Compound* ***2****).* From 2,3-dichloro-1,4-naphthoquinone and (*E*)-1-(3-aminophenyl)-3-(2,3,4-trimethoxyphenyl)prop-2-en-1-one. Castle red solid. 51% yield; mp 175−176 °C; IR (neat) cm$^{-1}$: 3299, 1672, 1593, 1567. $^1$H NMR (300 MHz, DMSO-$d_6$): δ 3.77, 3.86 (2 s, 9H, 3 × $OCH_3$), 6.92 (d, *J* = 8.9 Hz, 1H, Ar*H*), 7.40 (d, *J* = 7.9 Hz, 1H, Ar*H*), 7.51 (t, *J* = 7.8 Hz, 1H, Ar*H*), 7.73 (d, *J* = 8.8 Hz, 1H, Ar*H*), 7.76 (d, *J* = 15.7 Hz, 1H, COC*H*═CHAr), 7.82−7.93 (m, 5H, Ar*H*, COCH═C*H*Ar), 8.05 (d, *J* = 8.0 Hz, 2H, Ar*H*), 9.49 (s, 1H, N*H*). $^{13}$C NMR (75 MHz, DMSO-$d_6$): δ 56.1, 60.5, 61.5, 108.5, 115.2, 120.5, 120.9, 123.2, 123.7, 124.2, 126.1, 126.6, 127.9, 128.4, 130.4, 131.9, 133.3, 134.8, 137.7, 138.8, 139.5, 141.8, 143.1, 153.2, 155.9, 176.8, 180.0, 188.9. HRMS-TOF: [M + H]$^+$, 504.1198 (calcd for $C_{28}H_{23}ClNO_6$: 504.1208).

*(E)-2-Chloro-3-((3-(3-(3,4,5-trimethoxyphenyl)acryloyl)-phenyl)amino)naphthalene-1,4-dione (Compound* ***3****).* From 2,3-dichloro-1,4-naphthoquinone and (*E*)-1-(3-aminophenyl)-3-(3,4,5-trimethoxyphenyl)prop-2-en-1-one. Castle red solid. 38% yield; mp 213−215 °C; IR (neat) cm$^{-1}$: 3295, 1668, 1603, 1574. $^1$H NMR (500 MHz, DMSO-$d_6$): δ 3.71, 3.84 (2 s, 9H, 3 × $OCH_3$), 7.20 (s, 2H, Ar*H*), 7.43 (dd, *J* = 7.8, 1.1 Hz, 1H, Ar*H*), 7.52 (t, *J* = 7.8 Hz, 1H, Ar*H*), 7.69 (d, *J* = 15.6 Hz, 1H, COC*H*═CHAr), 7.79−7.83 (m, 3H, Ar*H*, COCH═C*H*Ar), 7.86−7.91 (m, 2H, Ar*H*), 8.05 (d, *J* = 7.7 Hz, 2H, Ar*H*), 9.45 (s, 1H, N*H*). $^{13}$C NMR (125 MHz, DMSO-$d_6$): δ 56.2, 60.2, 106.6, 115.4, 121.4, 123.2, 124.3, 126.2, 126.6, 128.0, 128.5, 130.2, 130.4, 132.0, 133.3, 134.8, 137.6, 139.6, 139.9, 143.2, 144.7, 153.2, 176.9, 180.1, 189.0. HRMS-TOF: [M + H]$^+$, 504.1199 (calcd for $C_{28}H_{23}ClNO_6$: 504.1208).

*(E)-2-Chloro-3-((3-(3-(4-hydroxy-3,5-dimethoxyphenyl)-acryloyl)phenyl)amino)naphthalene-1,4-dione (Compound* ***4****).* From 2,3-dichloro-1,4-naphthoquinone and (*E*)-1-(3-aminophenyl)-3-(4-hydroxy-3,5-dimethoxyphenyl)prop-2-en-1-one. Orange solid. 35% yield; mp 199−201 °C; IR (neat) cm$^{-1}$: 3300, 1671, 1594, 1567. $^1$H NMR (500 MHz, DMSO-$d_6$): δ 3.83 (2 s, 6H, 2 × $OCH_3$), 7.16 (s, 2H, Ar*H*), 7.41 (dd, *J* = 7.9, 1.2 Hz, 1H, Ar*H*), 7.51 (t, *J* = 7.8 Hz, 1H, Ar*H*), 7.67 (d, *J* = 15.5 Hz, 1H, COC*H*═CHAr), 7.71 (d, *J* = 15.5 Hz, 1H, COCH═C*H*Ar), 7.81−7.83 (m, 2H, Ar*H*), 7.86−7.90 (m, 2H, Ar*H*), 8.05 (d, *J* = 7.4 Hz, 2H, Ar*H*), 9.12 (br s, 1H, O*H*), 9.43 (br s, 1H, N*H*). $^{13}$C NMR (125 MHz, DMSO-$d_6$): δ 56.2, 107.0, 115.3, 119.2, 123.2, 124.3, 125.0, 126.2, 126.6, 127.8, 128.4, 130.4, 132.0, 133.4, 134.8, 137.9, 138.9, 139.5, 143.2, 145.5, 148.1, 176.9, 180.1, 188.8. HRMS-TOF: [M + H]$^+$, 490.1047 (calcd for $C_{27}H_{21}ClNO_6$: 490.1052).

*(E)-2-Chloro-3-((3-(3-(4-hydroxyphenyl)acryloyl)phenyl)-amino)naphthalene-1,4-dione (Compound* ***5****).* From 2,3-dichloro-1,4-naphthoquinone and (*E*)-1-(3-aminophenyl)-3-(4-hydroxyphenyl)prop-2-en-1-one. Red wine solid. 45% yield; mp 235−236 °C; IR (neat) cm$^{-1}$: 3296, 1675, 1596, 1567. $^1$H NMR (500 MHz, DMSO-$d_6$): δ 6.83 (d, *J* = 8.6 Hz, 2H, Ar*H*), 7.39 (d, *J* = 7.8 Hz, 1H, Ar*H*), 7.50 (t, *J* = 7.9 Hz, 1H, Ar*H*), 7.64 (d, *J* = 15.6 Hz, 1H, COC*H*═CHAr), 7.69 (d, *J* = 15.0 Hz, 1H, COCH═C*H*Ar), 7.68 (d, *J* = 8.6 Hz, 2H, Ar*H*), 7.80−7.83 (m, 2H, Ar*H*), 7.86−7.89 (m, 2H, Ar*H*), 8.05 (d, *J* = 7.7 Hz, 2H, Ar*H*), 9.44 (s, 1H, N*H*), 10.13 (s, 1H, O*H*). $^{13}$C NMR (125 MHz, DMSO-$d_6$): δ 115.1, 115.9, 118.5, 123.3, 124.3, 125.8, 126.2, 126.6, 127.9, 128.4, 130.4, 131.1, 132.0, 133.3, 134.8, 137.9, 139.5, 143.2, 144.8, 160.2, 176.9, 180.0, 188.8. HRMS-TOF: [M + H]$^+$, 430.0828 (calcd for $C_{25}H_{17}ClNO_4$: 430.0841).

*(E)-2-Chloro-3-((4-(3-(3-(3-methoxyphenyl)acryloyl)phenyl)-amino)naphthalene-1,4-dione (Compound* ***6****).* From 2,3-dichloro-1,4-naphthoquinone and (*E*)-1-(4-aminophenyl)-3-(3-methoxyphenyl)prop-2-en-1-one. Red solid. 41% yield; mp 210−212 °C; IR (neat) cm$^{-1}$: 3223, 1676, 1596, 1568. $^1$H NMR (500 MHz, DMSO-$d_6$): δ 3.83 (s, 3H, $OCH_3$), 7.02 (dd, *J* = 8.1, 2.1 Hz, 1H, Ar*H*), 7.23 (d, *J* = 8.6 Hz, 2H, Ar*H*), 7.37 (t, *J* = 8.0 Hz, 1H, Ar*H*), 7.44 (d, *J* = 7.6 Hz, 1H, Ar*H*), 7.49 (s, 1H, Ar*H*), 7.70 (d, *J* = 15.5 Hz, 1H, COC*H*═CHAr), 7.84 (t, *J* = 7.5 Hz, 1H, Ar*H*), 7.89 (t, *J* = 7.5 Hz, 1H, Ar*H*), 7.98 (d, *J* = 15.6 Hz, 1H, COCH═C*H*Ar), 8.06 (d, *J* = 7.5 Hz, 2H, Ar*H*), 8.14 (d, *J* = 8.7 Hz, 2H, Ar*H*), 9.59 (s, 1H, N*H*). $^{13}$C NMR (125 MHz, DMSO-$d_6$): δ 55.3, 113.3, 116.6, 118.9, 121.7, 121.9, 122.3, 126.3, 126.6, 129.0, 130.0, 130.6, 131.8, 132.2, 133.6, 134.8, 136.2, 142.6, 143.3, 143.9, 159.7, 177.1, 180.0, 187.6. HRMS-TOF: [M + H]$^+$, 444.1001 (calcd for $C_{26}H_{19}ClNO_4$: 444.0998).

*(E)-2-Chloro-3-((4-(3-(3,4-dimethoxyphenyl)acryloyl)-phenyl)amino)naphthalene-1,4-dione (Compound* ***7****).* From 2,3-dichloro-1,4-naphthoquinone and (*E*)-1-(4-aminophenyl)-3-(3,4-dimethoxyphenyl)prop-2-en-1-one. Red solid. 45% yield; mp 214−215 °C; IR (neat) cm$^{-1}$: 3227, 1674, 1593, 1574. $^1$H NMR (500 MHz, DMSO-$d_6$): δ 3.82, 3.86 (2 s, 6H, 2 × $OCH_3$), 7.02 (d, *J* = 8.4 Hz, 1H, Ar*H*), 7.22 (d, *J* = 8.6 Hz, 2H, Ar*H*), 7.38 (d, *J* = 8.3 Hz, 1H, Ar*H*), 7.54 (s, 1H, Ar*H*), 7.69 (d, *J* = 15.4 Hz, 1H, COC*H*═CHAr), 7.83 (dt, *J* = 7.5, 1.0 Hz, 1H, Ar*H*), 7.85 (d, *J* = 15.3 Hz, 1H, COCH═C*H*Ar), 7.89 (dt, *J* = 7.4, 1.0 Hz, 1H, Ar*H*), 8.05 (dd, *J* = 7.4, 1.1 Hz, 1H, Ar*H*), 8.06 (dd, *J* = 7.6, 1.0 Hz, 1H, Ar*H*), 8.12 (d, *J* = 8.6 Hz, 2H, Ar*H*), 9.57 (s, 1H, N*H*). $^{13}$C NMR (125 MHz, DMSO-$d_6$): δ 55.7, 55.8, 110.7, 111.6, 118.6, 119.6, 122.0, 124.0, 126.3, 126.7, 127.7, 128.9, 130.6, 131.9, 132.6, 133.6, 134.8, 142.8, 143.8, 143.9, 149.1, 151.3, 177.0, 180.1, 187.5. HRMS-TOF: [M + H]$^+$, 474.1097 (calcd for $C_{27}H_{21}ClNO_5$: 474.1103).

*(E)-2-Chloro-3-((4-(3-(3,4,5-trimethoxyphenyl)acryloyl)-phenyl)amino)naphthalene-1,4-dione (Compound* ***8****).* From 2,3-dichloro-1,4-naphthoquinone and (*E*)-1-(4-aminophenyl)-3-(3,4,5-trimethoxyphenyl)prop-2-en-1-one. Orange solid. 44% yield; mp 213−214 °C; IR (neat) cm$^{-1}$: 3296, 1673, 1591, 1569. $^1$H NMR (500 MHz, DMSO-$d_6$): δ 3.71, 3.86 (2 s, 9H, 3 × $OCH_3$), 7.22−7.24 (m, 4H, Ar*H*), 7.68 (d, *J* = 15.5 Hz, 1H, COC*H*═CHAr), 7.84 (dt, *J* = 7.5, 1.1 Hz, 1H, Ar*H*), 7.89 (dt, *J* = 7.5, 1.3 Hz, 1H, Ar*H*), 7.92 (d, *J* = 15.6 Hz, 1H, COCH═C*H*Ar), 8.06 (dd, *J* = 7.6, 1.3 Hz, 1H, Ar*H*), 8.07 (dd, *J* = 7.3, 1.2 Hz, 1H, Ar*H*), 8.14 (d, *J* = 8.7 Hz, 2H, Ar*H*), 9.61 (s, 1H, N*H*). $^{13}$C NMR (125 MHz, DMSO-$d_6$): δ 56.2, 60.2, 106.5, 118.7, 121.2, 122.0, 126.3, 126.7, 129.0, 130.4, 130.6, 131.9, 132.4, 133.6, 134.8, 139.7, 142.7, 143.9, 144.0, 153.2, 177.1, 180.0, 187.5. HRMS-TOF: [M + H]$^+$, 504.1192 (calcd for $C_{28}H_{23}ClNO_6$: 504.1208).

*(E)-2-Chloro-3-((4-(3-(3-hydroxy-4-methoxyphenyl)-acryloyl)phenyl)amino)naphthalene-1,4-dione (Compound*


https://doi.org/10.1021/acsomega.3c03176
ACS Omega 2023, 8, 32593−32605

*9*). From 2,3-dichloro-1,4-naphthoquinone and (*E*)-1-(4-aminophenyl)-3-(3-hydroxy-4-methoxyphenyl)prop-2-en-1-one. Castle red solid. 58% yield; mp 218 °C (d); IR (neat) $cm^{-1}$: 3534, 3290, 1676, 1590, 1563. $^1H$ NMR (300 MHz, DMSO-$d_6$): $\delta$ 3.84 (s, 3H, $OCH_3$), 7.00 (d, $J$ = 8.3 Hz, 1H, Ar*H*), 7.22 (d, $J$ = 8.6 Hz, 2H, Ar*H*), 7.30 (d, $J$ = 8.5 Hz, 1H, Ar*H*), 7.32 (s, 1H, Ar*H*), 7.60 (d, $J$ = 15.4 Hz, 1H, COC*H*═CHAr), 7.73 (d, $J$ = 15.5 Hz, 1H, COCH═C*H*Ar), 7.84 (t, $J$ = 7.6 Hz, 1H, Ar*H*), 7.89 (t, $J$ = 7.5 Hz, 1H, Ar*H*), 8.05−8.11 (m, 4H, Ar*H*), 9.16 (s, 1H, O*H*), 9.57 (s, 1H, N*H*). $^{13}C$ NMR (75 MHz, DMSO-$d_6$): $\delta$ 55.7, 112.0, 114.9, 118.5, 119.4, 121.9, 122.0, 126.2, 126.6, 127.8, 128.7, 130.5, 131.8, 132.6, 133.5, 134.7, 142.6, 143.6, 143.8, 146.6, 150.2, 176.9, 179.9, 187.4. HRMS-TOF: $[M + H]^+$, 460.0946 (calcd for $C_{26}H_{19}ClNO_5$: 460.0946).

*(E)-2-Chloro-3-((4-(3-(4-hydroxyphenyl)acryloyl)phenyl)-amino)naphthalene-1,4-dione (Compound **10**)*. From 2,3-dichloro-1,4-naphthoquinone and (*E*)-1-(4-aminophenyl)-3-(4-hydroxyphenyl)prop-2-en-1-one. Red wine solid. 43% yield; mp 250 °C (d); IR (neat) $cm^{-1}$: 3224, 1675, 1593, 1569. $^1H$ NMR (500 MHz, DMSO-$d_6$): $\delta$ 6.83 (d, $J$ = 8.6 Hz, 2H, Ar*H*), 7.22 (d, $J$ = 8.7 Hz, 2H, Ar*H*), 7.66 (d, $J$ = 15.4 Hz, 1H, COC*H*═CHAr), 7.73 (d, $J$ = 8.6 Hz, 2H, Ar*H*), 7.75 (d, $J$ = 15.4 Hz, 1H, COCH═C*H*Ar), 7.84 (dt, $J$ = 7.5, 1.2 Hz, 1H, Ar*H*), 7.89 (dt, $J$ = 7.5, 1.3 Hz, 1H, Ar*H*), 8.05−8.09 (m, 4H, Ar*H*), 9.56 (s, 1H, N*H*), 10.09 (s, 1H, O*H*). $^{13}C$ NMR (125 MHz, DMSO-$d_6$): $\delta$ 115.9, 118.5, 118.5, 122.1, 126.0, 126.3, 126.6, 128.7, 130.6, 131.0, 131.8, 132.7, 133.6, 134.8, 142.7, 143.6, 143.9, 160.0, 177.1, 180.0, 187.5. HRMS-TOF: $[M + H]^+$, 430.0830 (calcd for $C_{25}H_{17}ClNO_4$: 430.0841).

**Cytotoxicity Assay.** The cells suspended in the corresponding culture medium were inoculated onto the 96-well microtiter plates (Corning, Inc., NY, USA) at a density of 10,000−20,000 cells per well and incubated for 24 h at 37 °C in a humidified atmosphere with 95% air and 5% $CO_2$. An equal volume of additional medium containing either the serial dilutions of the test compounds, positive control (etoposide and/or doxorubicin), or negative control (DMSO) was added to the desired final concentrations, and the microtiter plates were further incubated for an additional 48 h. The number of surviving cells in each well was determined using the MTT assay[49,50] (for HuCCA-1, HepG2, A549, T47D, MDA-MB-231, and MRC-5 cells) and the XTT assay[51] (for MOLT-3 cells). The $IC_{50}$ value is defined as the drug (or compound) concentration that inhibits cell growth by 50% (relative to the negative control).

**ADP-Glo Kinase Assay.** The FGFR kinase inhibitory activity of the target compounds was evaluated using the ADP-Glo kinase assay (Promega, Wisconsin, USA). Briefly, 8 $\mu$L of buffer (200 mM Tris−HCl pH 7.5, 100 mM $MgCl_2$, and 0.5 mg/mL bovine serum albumin) was initially added to a 384-well plate. After that, 5 $\mu$L of the FGFR1 enzyme (1.25 ng/$\mu$L, Millipore, Billerica, MA, Cat. N.14−582) and 2 $\mu$L of inhibitors were added. Then, 10 $\mu$L of a mixture of 12.5 $\mu$g/mL poly(glu-tyr) and 25 $\mu$M ATP was added, and the plate was incubated at room temperature for 1 h. To terminate the kinase reaction, 5 $\mu$L of the ADP-Glo reagent was then added and incubated for 40 min. Finally, 10 $\mu$L of the kinase detection reagent was added, and the plate was further incubated at room temperature for 30 min. The luminescence was detected using a microplate reader (Infinite M200 microplate reader, Tecan, Männedorf, Switzerland). All assays were performed in triplicate. The relative inhibition (%) of inhibitors was calculated in comparison to the control with no inhibitor as shown in eq 1.

$$\%\text{relative inhibition} = \frac{[(\text{positive} - \text{negative}) - (\text{sample} - \text{negative})]}{(\text{positive} - \text{negative})} \times 100 \quad (1)$$

**Computational Details.** *System Preparation.* The crystal structure of FGFR1 complexed with pemigatinib (PDB ID 7WCL)[52] was downloaded from the Protein Data Bank (PDB). The protonation state of all ionizable amino acids was determined at pH 7.4 using PROPKA 3.1.[53] The 3D chemical structures of the selected compounds (**5**, **7**, and **9**) were constructed using the Gaussian 09 program,[54] whereas that of the reference inhibitor, AZD4547, was obtained from PDB entry 4V05.[55] The protonation state of all studied ligands was determined at pH 7.4 using the MarvinSketch program.[56] All of the ligands were fully optimized using the Gaussian 09 program with the HF/6−31d level of theory.[57] Molecular docking simulation was performed by the CDOCKER module[58] implemented in the Discovery Studio 2.5 program using the site of pemigatinib in the FGFR1 crystal structure as a docking sphere (13 Å). The docked complexes with the lowest CDOCKER interaction energy of each system were chosen as the initial structure for MD simulation. The semi-empirical AM1-BCC charge model was used for the preparation of partial atomic charges and parameters of the ligands. The general AMBER force field version 2 (GAFF2)[59] and the AMBER ff14SB[60] force fields were applied for ligands and protein, respectively. All missing hydrogen atoms of FGFR1 were added using the LEaP module. Then, each system was solvated in a simulation box of the TIP3P water model[61] with a minimum buffer thickness of 12 Å followed by the incorporation of sodium counterions to keep the whole system neutral. To remove the bad contacts, the added hydrogen atoms and water molecules were subsequently minimized using 1500 steps of the steepest descent (SD) method followed by 1500 steps of conjugated gradient (CG) algorithm. Finally, the whole complex was minimized using the same procedure of SD and CG.

*Molecular Dynamics (MD) Simulation.* MD simulations of the FGFR1−ligand complexes in an aqueous solution were performed using the AMBER20 software package.[62] The SHAKE algorithm was used to constrain all covalent bonds involving hydrogen atoms,[63] allowing a 2 fs time step of integration. A 10 Å cutoff distance was set for nonbonded interactions,[64,65] while the long-range electrostatic interactions were treated using the particle mesh Ewald's summation approach.[66] Temperature and pressure were controlled by a Langevin thermostat and a Berendsen barostat, respectively. Initially, each system was thermalized from 10 to 310 K over 100 ps using the canonical ensemble (NVT) with positional restraints of 10.0 kcal/mol·Å$^2$ to the protein−ligand complex. Subsequently, the entire system was run under the isothermal−isobaric (NPT) ensemble (310 K and 1 atm) MD simulation until 50 ns was reached.

*Structural Analysis and Free Energy Calculation.* The CPPTRAJ module[67] of AMBER20 was used to compute structural information, including root-mean-square displacement (RMSD), the number of native and non-native contacts (# contacts), and solvent-accessible surface area (SASA). The per-residue decomposition free energy ($\Delta G_{bind,res}$) and energy contribution were calculated using the molecular mechanics/


https://doi.org/10.1021/acsomega.3c03176
ACS Omega 2023, 8, 32593−32605

generalized Born surface area (MM/GBSA) method[68] on 200 frames extracted from the last 20 ns of the MD production phase.

*Druglikeness Prediction.* Druglike properties of the three compounds (**5**, **7**, and **9**) with potent FGFR1 inhibitory effects as well as the known inhibitor (AZD4547) were predicted using the SwissADME web tool.[48]

## ■ ASSOCIATED CONTENT

### Supporting Information

The Supporting Information is available free of charge at https://pubs.acs.org/doi/10.1021/acsomega.3c03176.

FGFR1 tyrosine kinase inhibitory activity of naphthoquinone−chalcone hybrids **1**−**10** and AZD4547, $^{1}$H and $^{13}$C NMR spectra of compounds **1**−**10**, and chromatographic purity analysis of compounds **1**−**10** using high-performance liquid chromatography (HPLC) (PDF)

## ■ AUTHOR INFORMATION


### Corresponding Authors

**Panupong Mahalapbutr** − *Department of Biochemistry, Center for Translational Medicine, Faculty of Medicine, Khon Kaen University, Khon Kaen 40002, Thailand;* orcid.org/0000-0003-4389-334X; Email: panupma@kku.ac.th

**Ratchanok Pingaew** − *Department of Chemistry, Faculty of Science, Srinakharinwirot University, Bangkok 10110, Thailand;* orcid.org/0000-0003-4977-5854; Phone: +66-2-649-5000 ext. 18253; Email: ratchanok@g.swu.ac.th; Fax: 662-260-0128

### Authors

**Ronnakorn Leechaisit** − *Department of Chemistry, Faculty of Science, Srinakharinwirot University, Bangkok 10110, Thailand*

**Pornthip Boonsri** − *Department of Chemistry, Faculty of Science, Srinakharinwirot University, Bangkok 10110, Thailand*

**Kun Karnchanapandh** − *Program in Bioinformatics and Computational Biology, Graduate School and Structural and Computational Biology Research Unit, Department of Biochemistry, Faculty of Science, Chulalongkorn University, Bangkok 10330, Thailand*

**Thanyada Rungrotmongkol** − *Program in Bioinformatics and Computational Biology, Graduate School and Structural and Computational Biology Research Unit, Department of Biochemistry, Faculty of Science, Chulalongkorn University, Bangkok 10330, Thailand*

**Veda Prachayasittikul** − *Center for Research Innovation and Biomedical Informatics, Faculty of Medical Technology, Mahidol University, Bangkok 10700, Thailand;* orcid.org/0000-0001-6338-3721

**Supaluk Prachayasittikul** − *Center for Research Innovation and Biomedical Informatics, Faculty of Medical Technology, Mahidol University, Bangkok 10700, Thailand*

**Somsak Ruchirawat** − *Laboratory of Medicinal Chemistry, Chulabhorn Research Institute, Bangkok 10210, Thailand; Program in Chemical Sciences, Chulabhorn Graduate Institute, Bangkok 10210, Thailand; Center of Excellence on Environmental Health and Toxicology (EHT), Commission on Higher Education, Ministry of Education, Bangkok 10400, Thailand*

**Virapong Prachayasittikul** − *Department of Clinical Microbiology and Applied Technology, Faculty of Medical Technology, Mahidol University, Bangkok 10700, Thailand*

Complete contact information is available at: https://pubs.acs.org/10.1021/acsomega.3c03176


### Notes

The authors declare no competing financial interest.

## ■ ACKNOWLEDGMENTS

This work was supported by the Srinakharinwirot University and National Science, Research and Innovation Fund (NSRF) (grant no. 029/2565). P.M. thanks the Fundamental Fund of Khon Kaen University for financial support. Veda P. is supported by Mahidol University (Basic Research Fund: fiscal year 2022). We thank Miss Sasiwimon Lalitmanat, Center for Research Innovation and Biomedical Informatics, Faculty of Medical Technology, Mahidol University, for HPLC analysis. We are grateful to the Chulabhorn Research Institute for bioactivity testing and HRMS measurements.

## ■ REFERENCES


(1) Sung, H.; Ferlay, J.; Siegel, R. L.; Laversanne, M.; Soerjomataram, I.; Jemal, A.; Bray, F. Global Cancer Statistics 2020: GLOBOCAN estimates of incidence and mortality worldwide for 36 cancers in 185 countries. *CA Cancer J. Clin.* **2021**, *71*, 209−249.

(2) Wang, X.; Zhang, H.; Chen, X. Drug resistance and combating drug resistance in cancer. *Cancer Drug Resist.* **2019**, *2*, 141−160.

(3) Carugo, A.; Draetta, G. F. Academic discovery of anticancer drugs: Historic and future perspectives. *Annu. Rev. Cancer Biol.* **2018**, *3*, 385−408.

(4) Nass, S. J.; Rothenberg, M. L.; Pentz, R.; Hricak, H.; Abernethy, A.; Anderson, K.; Gee, A. W.; Harvey, R. D.; Piantadosi, S.; Bertagnolli, M. M.; Schrag, D.; Schilsky, R. L. Accelerating anticancer drug development - opportunities and trade-offs. *Nat. Rev. Clin. Oncol.* **2018**, *15*, 777−786.

(5) Hait, W. N.; Lebowitz, P. F. Moving upstream in anticancer drug development. *Nat. Rev. Drug Discovery* **2019**, *18*, 159−160.

(6) Kommalapati, A.; Tella, S. H.; Borad, M.; Javle, M.; Mahipal, A. FGFR inhibitors in oncology: insight on the management of toxicities in clinical practice. *Cancers* **2021**, *13*, 2968.

(7) Weaver, A.; Bossaer, J. B. Fibroblast growth factor receptor (FGFR) inhibitors: A review of a novel therapeutic class. *J. Oncol. Pharm. Pract.* **2021**, *27*, 702−710.

(8) Dai, S.; Zhou, Z.; Chen, Z.; Xu, G.; Chen, Y. Fibroblast growth factor receptors (FGFRs): Structures and small molecule inhibitors. *Cell* **2019**, *8*, 614.

(9) Katoh, M. Therapeutics targeting FGF signaling network in human diseases. *Trends Pharmacol. Sci.* **2016**, *37*, 1081−1096.

(10) Zheng, J.; Zhang, W.; Li, L.; He, Y.; Wei, Y.; Dang, Y.; Nie, S.; Guo, Z. Signaling pathway and small-molecule drug discovery of FGFR: A comprehensive review. *Front. Chem.* **2022**, *10*, No. 860985.

(11) Meunier, B. Hybrid molecules with a dual mode of action: dream or reality? *Acc. Chem. Res.* **2008**, *41*, 69−77.

(12) Nepali, K.; Sharma, S.; Sharma, M.; Bedi, P. M. S.; Dhar, K. L. Rational approaches, design strategies, structure activity relationship and mechanistic insights for anticancer hybrids. *Eur. J. Med. Chem.* **2014**, *77*, 422−487.

(13) Shaveta; Mishra, S.; Singh, P. Hybrid molecules: The privileged scaffolds for various pharmaceuticals. *Eur. J. Med. Chem.* **2016**, *124*, 500−536.

(14) Xu, Z.; Zhao, S. J.; Liu, Y. 1,2,3-Triazole-containing hybrids as potential anticancer agents: Current developments, action mechanisms and structure-activity relationships. *Eur. J. Med. Chem.* **2019**, *183*, 111700.

(15) Szumilak, M.; Wiktorowska-Owczarek, A.; Stanczak, A. Hybrid drugs-A strategy for overcoming anticancer drug resistance? *Molecules* **2021**, *26*, 2601.
(16) Shalini; Kumar, V. Have molecular hybrids delivered effective anti-cancer treatments and what should future drug discovery focus on? *Expert Opin. Drug Discovery* **2021**, *16*, 335−363.
(17) Zhuang, C.; Zhang, W.; Sheng, C.; Zhang, W.; Xing, C.; Miao, Z. Chalcone: A privileged structure in medicinal chemistry. *Chem. Rev.* **2017**, *117*, 7762−7810.
(18) Gomes, M. N.; Muratov, E. N.; Pereira, M.; Peixoto, J. C.; Rosseto, L. P.; Cravo, P. V. L.; Andrade, C. H.; Neves, B. J. Chalcone derivatives: Promising starting points for drug design. *Molecules* **2017**, *22*, 1210.
(19) Sahu, N. K.; Balbhadra, S. S.; Choudhary, J.; Kohli, D. V. Exploring pharmacological significance of chalcone scaffold: A review. *Curr. Med. Chem.* **2012**, *19*, 209−225.
(20) Batovska, D. I.; Todorova, I. T. Trends in utilization of the pharmacological potential of chalcones. *Curr. Clin. Pharmacol.* **2010**, *5*, 1−29.
(21) Zhou, B.; Xing, C. Diverse molecular targets for chalcones with varied bioactivities. *Med. Chem.* **2015**, *5*, 388−404.
(22) Mahapatra, D. K.; Bharti, S. K.; Asati, V. Anti-cancer chalcones: Structural and molecular target perspectives. *Eur. J. Med. Chem.* **2015**, *98*, 69−114.
(23) El-Najjar, N.; Gali-Muhtasib, H.; Ketola, R. A.; Vuorela, P.; Urtti, A.; Vuorela, H. The chemical and biological activities of quinones: overview and implications in analytical detection. *Phytochem. Rev.* **2011**, *10*, 353.
(24) Sunassee, S. N.; Davies-Coleman, M. T. Cytotoxic and antioxidant marine prenylated quinones and hydroquinones. *Nat. Prod. Rep.* **2012**, *29*, 513−535.
(25) Martinellp, M.; Stefanp, V.; Gerbase, A. E.; Farias, M. Synthesis of 5-dodecanoylamine-8-hydroxy-1,4-naphthoquinone and study of some of its bivalent metal chelates. *J. Coord. Chem.* **1999**, *48*, 529−539.
(26) Hillard, E. A.; de Abreu, F. C.; Ferreira, D. C. M.; Jaouen, G.; Goulart, M. O. F.; Amatore, C. Electrochemical parameters and techniques in drug development, with an emphasis on quinones and related compounds. *Chem. Commun.* **2008**, *23*, 2612−2628.
(27) O'Brien, P. J. Molecular mechanisms of quinone cytotoxicity. *Chem.-Biol. Interact.* **1991**, *80*, 1−41.
(28) Benites, J.; Valderrama, J. A.; Bettega, K.; Pedrosa, R. C.; Calderon, P. B.; Verrax, J. Biological evaluation of donor-acceptor aminonaphthoquinones as antitumor agents. *Eur. J. Med. Chem.* **2010**, *45*, 6052−6057.
(29) Gao, F.; Huang, G.; Xiao, J. Chalcone hybrids as potential anticancer agents: Current development, mechanism of action, and structure-activity relationship. *Med. Res. Rev.* **2020**, *40*, 2049−2084.
(30) Mohamed, M. F. A.; Abuo-Rahma, G. E.-D. A. Molecular targets and anticancer activity of quinoline−chalcone hybrids: literature review. *RSC Adv.* **2020**, *10*, 31139−31155.
(31) Thakur, G. A.; Kadu, R. K.; Patil, V. R.; Thakur, P. B. Progress in the synthesis of oxindole-naphthoquinone molecular hybrid scaffolds: A concise review. *ChemistrySelect* **2020**, *5*, 13628−13643.
(32) Patel, O. P. S.; Beteck, R. M.; Legoabe, L. J. Antimalarial application of quinones: A recent update. *Eur. J. Med. Chem.* **2021**, *210*, No. 113084.
(33) Viswanathan, G. K.; Paul, A.; Gazit, E.; Segal, D. Naphthoquinone tryptophan hybrids: A promising small molecule scaffold for mitigating aggregation of amyloidogenic proteins and peptides. *Front. Cell Dev. Biol.* **2019**, *7*, 242.
(34) Pingaew, R.; Prachayasittikul, V.; Worachartcheewan, A.; Nantasenamat, C.; Prachayasittikul, S.; Ruchirawat, S.; Prachayasittikul, V. Novel 1,4-naphthoquinone-based sulfonamides: Synthesis, QSAR, anticancer and antimalarial studies. *Eur. J. Med. Chem.* **2015**, *103*, 446−459.
(35) Sooknual, P.; Pingaew, R.; Phopin, K.; Ruankham, W.; Prachayasittikul, S.; Ruchirawat, S.; Prachayasittikul, V. Synthesis and neuroprotective effects of novel chalcone-triazole hybrids. *Bioorg. Chem.* **2020**, *105*, No. 104384.
(36) Nguyen, H.-T.; Dang Thi, T. A.; Hoang Thi, P.; Le-Nhat-Thuy, G.; Nguyen Thi, Q. G.; Nguyen Tuan, A.; Le Thi, T. A.; Van Nguyen, T. A new approach for the synthesis of novel naphthoquinone chalcone hybrid compounds. *Tetrahedron Lett.* **2021**, *81*, No. 153337.
(37) Kolundžija, B.; Marković, V.; Stanojković, T.; Joksović, L.; Matić, I.; Todorović, N.; Nikolić, M.; Joksović, M. D. Novel anthraquinone based chalcone analogues containing an imine fragment: synthesis, cytotoxicity and anti-angiogenic activity. *Bioorg. Med. Chem. Lett.* **2014**, *24*, 65−71.
(38) Qiu, H.-Y.; Wang, F.; Wang, X.; Sun, W.-X.; Qi, J.-L.; Pang, Y.-J.; Yang, R.-W.; Lu, G.-H.; Wang, X.-M.; Yang, Y.-H. Design, synthesis, and biological evaluation of chalcone-containing shikonin derivatives as inhibitors of tubulin polymerization. *ChemMedChem* **2017**, *12*, 399−406.
(39) Jardim, G. A. M.; Guimarães, T. T.; Pinto, M. d. C. F. R.; Cavalcanti, B. C.; de Farias, K. M.; Pessoa, C.; Gatto, C. C.; Nair, D. K.; Namboothiri, I. N. N.; da Silva Júnior, E. N. Naphthoquinone-based chalcone hybrids and derivatives: Synthesis and potent activity against cancer cell lines. *Med. Chem. Commun.* **2015**, *6*, 120−130.
(40) Adelusi, T. I.; Oyedele, A.-Q. K.; Boyenle, I. D.; Ogunlana, A. T.; Adeyemi, R. O.; Ukachi, C. D.; Idris, M. O.; Olaoba, O. T.; Adedotun, I. O.; Kolawole, O. E.; Xiaoxing, Y.; Abdul-Hammed, M. Molecular modeling in drug discovery. *Inf. Med. Unlocked* **2022**, *29*, No. 100880.
(41) Mahalapbutr, P.; Leechaisit, R.; Thongnum, A.; Todsaporn, D.; Prachayasittikul, V.; Rungrotmongkol, T.; Prachayasittikul, S.; Ruchirawat, S.; Prachayasittikul, V.; Pingaew, R. Discovery of anilino-1,4-naphthoquinones as potent EGFR tyrosine kinase inhibitors: Synthesis, biological evaluation, and comprehensive molecular modeling. *ACS Omega* **2022**, *7*, 17881−17893.
(42) Ganji, L. R.; Gandhi, L.; Musturi, V.; Kanyalkar, M. A. Design, synthesis, and evaluation of different scaffold derivatives against NS2B-NS3 protease of dengue virus. *Med. Chem. Res.* **2021**, *30*, 285−301.
(43) Çoban, G.; Aydın Köse, F. Synthesis, biological evaluations and molecular modelling studies of novel indolin-2-ones designing as FGFR inhibitors. *Saudi. Pharm. J.* **2019**, *27*, 952−967.
(44) Liu, Z.; Yu, S.; Chen, D.; Shen, G.; Wang, Y.; Hou, L.; Lin, D.; Zhang, J.; Ye, F. Design, synthesis, and biological evaluation of 3-vinyl-quinoxalin-2(1*H*)-one derivatives as novel antitumor inhibitors of FGFR1. *Drug Des. Dev. Ther.* **2016**, *10*, 1489−1500.
(45) Abdel-Mohsen, H. T.; Abd El-Meguid, E. A.; El Kerdawy, A. M.; Mahmoud, A. E. E.; Ali, M. M. Design, synthesis, and molecular docking of novel 2-arylbenzothiazole multiangiokinase inhibitors targeting breast cancer. *Arch. Pharm.* **2020**, *353*, 1900340.
(46) Volynets, G.; Vdovin, V.; Lukashov, S.; Borovykov, O.; Borysenko, I.; Gryshchenko, A.; Bdzhola, V.; Iatsyshyna, A.; Lukash, L.; Bilokin, Y.; Yarmoluk, S. Identification of novel indazole-based inhibitors of fibroblast growth factor receptor 1 (FGFR1). *Curr. Enzyme Inhib.* **2021**, *17*, 161−165.
(47) Pan, Y. L.; Liu, Y. L.; Chen, J. Z. Computational simulation studies on the binding selectivity of 1-(1H-benzimidazol-5-yl)-5-aminopyrazoles in complexes with FGFR1 and FGFR4. *Molecules* **2018**, *23*, 767.
(48) Daina, A.; Michielin, O.; Zoete, V. SwissADME: a free web tool to evaluate pharmacokinetics, drug-likeness and medicinal chemistry friendliness of small molecules. *Sci. Rep.* **2017**, *7*, 42717.
(49) Carmichael, J.; DeGraff, W. G.; Gazdar, A. F.; Minna, J. D.; Mitchell, J. B. Evaluation of a tetrazolium-based semiautomated colorimetric assay: assessment of chemosensitivity testing. *Cancer Res.* **1987**, *47*, 936−942.
(50) Denizot, F.; Lang, R. Rapid colorimetric assay for cell growth and survival: Modifications to the tetrazolium dye procedure giving improved sensitivity and reliability. *J. Immunol. Methods* **1986**, *89*, 271−277.
(51) Doyle, A.; Griffiths, J. B. *Mammalian cell culture : essential techniques*; John Wiley & Sons, 1997.


https://doi.org/10.1021/acsomega.3c03176
*ACS Omega* 2023, 8, 32593−32605

(52) Lin, Q.; Chen, X.; Qu, L.; Guo, M.; Wei, H.; Dai, S.; Jiang, L.; Chen, Y. Characterization of the cholangiocarcinoma drug pemigatinib against FGFR gatekeeper mutants. *Commun. Chem.* **2022**, *5*, 100.
(53) Olsson, M. H. M.; Søndergaard, C. R.; Rostkowski, M.; Jensen, J. H. PROPKA3: Consistent treatment of internal and surface residues in empirical pKa predictions. *J. Chem. Theory Comput.* **2011**, *7*, 525−537.
(54) Frisch, M. J.; Trucks, G. W.; Schlegel, H. B.; Scuseria, G. E.; Robb, M. A.; Cheeseman, J. R.; Scalmani, G.; Barone, V.; Mennucci, B.; Petersson, G. A.; Nakatsuji, H.; Caricato, M.; Li, X.; Hratchian, H. P.; Izmaylov, A. F.; Bloino, J.; Zheng, G.; Sonnenberg, J. L.; Hada, M.; Ehara, M.; Toyota, K.; Fukuda, R.; Hasegawa, J.; Ishida, M.; Nakajima, T.; Honda, Y.; Kitao, O.; Nakai, H.; Vreven, T.; J. A. J., Montgomery; Peralta, J. E.; Ogliaro, F.; Bearpark, M.; Heyd, J. J.; Brothers, E.; Kudin, K. N.; Staroverov, V. N.; Kobayashi, R.; Normand, J.; Raghavachari, K.; Rendell, A.; Burant, J. C.; Iyengar, S. S.; Tomasi, J.; Cossi, M.; Rega, N.; Millam, J. M.; Klene, M.; Knox, J. E.; Cross, J. B.; Bakken, V.; Adamo, C.; Jaramillo, J.; Gomperts, R.; Stratmann, R. E.; Yazyev, O.; Austin, A. J.; Cammi, R.; Pomelli, C.; Ochterski, J. W.; Martin, R. L.; Morokuma, K.; Zakrzewski, V. G.; Voth, G. A.; Salvador, P.; Dannenberg, J. J.; Dapprich, S.; Daniels, A. D.; Farkas, Ö.; Foresman, J. B.; Ortiz, J. V.; Cioslowski, J.; Fox, D. J. *gaussian 09, Revision d. 01*, Gaussian. Inc., Wallingford CT. 2009, *201*.
(55) Tucker, J. A.; Klein, T.; Breed, J.; Breeze, A. L.; Overman, R.; Phillips, C.; Norman, R. A. Structural insights into FGFR kinase isoform selectivity: diverse binding modes of AZD4547 and ponatinib in complex with FGFR1 and FGFR4. *Structure* **2014**, *22*, 1764−1774.
(56) Salvador, G. A.; Oteiza, P. I. Iron overload triggers redox-sensitive signals in human IMR-32 neuroblastoma cells. *Neurotoxicology* **2011**, *32*, 75−82.
(57) Mahalapbutr, P.; Lee, V. S.; Rungrotmongkol, T. Binding hotspot and activation mechanism of maltitol and lactitol toward the human sweet taste receptor. *J. Agric. Food Chem.* **2020**, *68*, 7974−7983.
(58) Wu, G.; Robertson, D. H., III; Vieth, M. Detailed analysis of grid-based molecular docking: A case study of CDOCKER−A CHARMm-based MD docking algorithm. *J. Comput. Chem.* **2003**, *24*, 1549−1562.
(59) Mahalapbutr, P.; Charoenwongpaiboon, T.; Phongern, C.; Kongtaworn, N.; Hannongbua, S.; Rungrotmongkol, T. Molecular encapsulation of a key odor-active 2-acetyl-1-pyrroline in aromatic rice with $\beta$-cyclodextrin derivatives. *J. Mol. Liq.* **2021**, *337*, No. 116394.
(60) Maier, J. A.; Martinez, C.; Kasavajhala, K.; Wickstrom, L.; Hauser, K. E.; Simmerling, C. ff14SB: Improving the accuracy of protein side chain and backbone parameters from ff99SB. *J. Chem. Theory Comput.* **2015**, *11*, 3696−3713.
(61) Jorgensen, W. L.; Chandrasekhar, J.; Madura, J. D.; Impey, R. W.; Klein, M. L. Comparison of simple potential functions for simulating liquid water. *J. Chem. Phys.* **1983**, *79*, 926−935.
(62) Salomon-Ferrer, R.; Case, D. A.; Walker, R. C. An overview of the AMBER biomolecular simulation package. *WIREs Comput. Mol. Sci.* **2013**, *3*, 198−210.
(63) Ryckaert, J.-P.; Ciccotti, G.; Berendsen, H. J. C. Numerical integration of the cartesian equations of motion of a system with constraints: molecular dynamics of n-alkanes. *J. Comput. Phys.* **1977**, *23*, 327−341.
(64) Chari, R.; Jerath, K.; Badkar, A. V.; Kalonia, D. S. Long- and short-range electrostatic interactions affect the rheology of highly concentrated antibody solutions. *Pharm. Res.* **2009**, *26*, 2607−2618.
(65) York, D. M.; Darden, T. A.; Pedersen, L. G. The effect of long-range electrostatic interactions in simulations of macromolecular crystals: A comparison of the Ewald and truncated list methods. *J. Chem. Phys.* **1993**, *99*, 8345−8348.
(66) Darden, T.; York, D.; Pedersen, L. Particle mesh Ewald: An *N*·log(*N*) method for Ewald sums in large systems. *J. Chem. Phys.* **1993**, *98*, 10089.
(67) Roe, D. R.; Cheatham, T. E., III PTRAJ and CPPTRAJ: Software for Processing and Analysis of Molecular Dynamics Trajectory Data. *J. Chem. Theory Comput.* **2013**, *9*, 3084−3095.
(68) Miller, B. R., III; McGee, T. D., Jr.; Swails, J. M.; Homeyer, N.; Gohlke, H.; Roitberg, A. E. *MMPBSA.py*: An efficient program for end-state free energy calculations. *J. Chem. Theory Comput.* **2012**, *8*, 3314−3321.


https://doi.org/10.1021/acsomega.3c03176
*ACS Omega* 2023, 8, 32593−32605